Grazing Incidence SANS and Reflectometry Combined with Simulation of Adsorbed Microgel Particles

Tetyana Kyrey[1,2] (t.kyrey@tu-berlin.de),
Marina Ganeva[2], Kornelia Gawlitza[3], Judith Witte[1], Regine von Klitzing[4], Olaf Soltwedel[5], Zhenyu Di[2], Stefan Wellert[1], Olaf Holderer[2]

[1]Technische Universität Berlin,
Stranski-Laboratory for Physical and Theoretical Chemistry,
Straße des 17. Juni 124, 10623 Berlin, Germany

[2]Jülich Centre for Neutron Science (JCNS) at Heinz Maier-Leibnitz Zentrum (MLZ),
Forschungszentrum Jülich GmbH,
Lichtenbergstraße 1, 85748 Garching, Germany

[3]BAM Federal Institute for Materials Research and Testing
Division 1.9 Chemical and Optical Sensing,
Richard-Willstätter-Straße 11, 12489 Berlin, Germany

[4] Technische Universität Darmstadt,
Fachbereich Physik, Fachgebiet Weiche Materie an Grenzflächen,
Alarich-Weiss-Strasse 10, 64287 Darmstadt, Germany

[5]Technische Universität München,
Lichtenbergstraße 1, 85748 Garching, Germany

Keywords: GISANS, Neutron Reflectometry, PEG microgels, BornAgain Simulation

ABSRTRACT

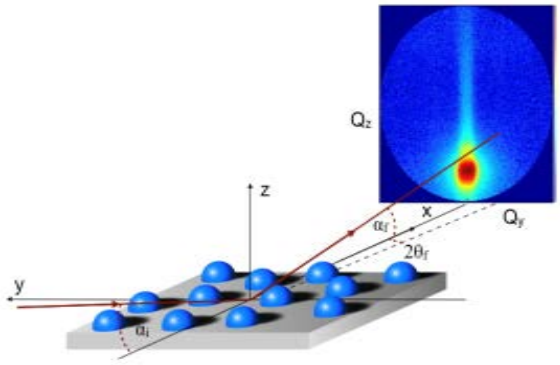

Adsorbed ethylene glycol based microgel particles on a silicon surface were studied. Neutron reflectometry (NR) and grazing incidence small-angle neutron scattering (GISANS) were performed to investigate their internal structure. Scattering experiments on soft matter systems such as adsorbed microgels often give only partial information about the inner structure of the polymer system. In this contribution, we discuss how the detailed inner structure of adsorbed microgel particles can be reconstructed by a combination of the specular Neutron Reflectivity (NR), Grazing Incidence Small Angle Neutron Scattering (GISANS) Atomic Force Microscopy (AFM) and a simulation in the framework of the Distorted Wave Born Approximation.

Keywords: Grazing incidence small-angle neutron scattering, neutron reflectometry, BornAgain simulation, adsorbed microgel particles

1. INTRODUCTION

Currently, fundamental research efforts are directed to the understanding of the interfacial properties of polymer architectures at solid surfaces. The confinement at a solid surface changes physical and chemical properties with respect to the corresponding bulk systems. Beside this, thin films are discussed as promising new materials for a variety of applications such as tuning of friction and lubrication properties, release of additives, adhesion promotion, and formation of hybrid bio-macromolecular assemblies or organic electronic devices [1-11]. Especially stimuli-responsive polymer coatings are of current interest, since they allow tune the underlying physical properties by an external trigger. Prominent examples for the investigated polymer systems are polymer brushes, cross linked brushes, thin hydrogel layers and adsorbed microgel particles [12-16].

The control of the surface functionalization requires the understanding of the physicochemical properties and the structure of the polymer architectures in the vicinity of the solid surfaces. The characterization of the lateral and vertical structure and the responsive behaviour is usually achieved by the use experimental techniques such as AFM and ellipsometry [17-21]. However, these methods do not allow direct measurements of the inner structure of the adsorbed polymer systems. In own turn such information can be achieves with the neutron and X-ray scattering methods [22-24]. Neutron reflectometry is one of the most popular methods for investigation of density profiles of the layered systems. It allows obtaining information about the structure in direction normal to surface. But the information about lateral features in this case is very limited or even absence. The other challenge of the investigation of the thin samples is their negligible amount on the surface. It demands the replacing of the transmission geometry on the grazing incidence geometry. In this case grazing incidence small angle neutron scattering (GISANS) is a powerful non-destructive method which gain access to a wider range of lateral and vertical structures and is sensitive to the morphology of the nanoscale objects at the surface or inside the thin film [25,26].

First experiments on adsorbed PNIPAM-co-AAc microgel particles, which are colloidal particles with an inner polymer network structure based on chemical cross-linking, showed no divergence of the correlation length of the thermally induced fluctuations of the polymer network at the volume phase transition temperature [27]. This is contrast to findings in the bulk phase, were the divergence could be detected by SANS. Probably, the presence of a solid surface strongly

influences the inner network fluctuations in the vicinity of the surface. Also, the inner dynamics of adsorbed microgel particles seems to be changed. The grazing incidence scattering technique in combination with neutron spin echo spectroscopy (GINSES) explores the near surface dynamics. With this method microgels based on the monomer 2-(2-methoxyethoxy)ethyl methacrylate (MeO_2MA), the comonomer poly(ethylene glycol) methyl ether methacrylate (OEGMA) and the cross-linker ethylene glycol dimethacrylate (EGDMA) were measured and a significant slowing down of the dynamics in immediate vicinity to the substrate was observed [28].
Grazing incidence techniques like GISANS and GINSES are challenging due to the combination of a complex scattering geometry compared to SANS or reflectometry and the various influences on the off-specular scattering signals. Hence, often the data treatment, analysis and interpretation are nontrivial. While the simulation of the bulk polymer system was done extensively [29-31], the simulation of adsorbed systems is still a challenging task. This contribution suggests a combination of experimental results obtained by GISANS and neutron reflectometry and numerical simulations as a potential approach.
In this paper, the investigation of the inner structure of adsorbed MeO_2MA-co-OEGMA microgels was studied. Because of the low cytotoxicity and immunogenicity [a], such microgels are a potential alternative for the synthesis of biocompatible microgels. Neutron reflectometry and GISANS measurements were performed and together with previous AFM results have been used for simulations of the experimental GISANS observations in the framework of the Distorted Wave Born Approximation by means of the BornAgain software package [32].

2. EXPERIMENTAL SECTION

2.1. Samples and Materials

Microgel particles based on the monomer 2-(2-methoxyethoxy)ethyl methacrylate (MeO_2MA), the comonomer poly(ethylene glycol) methyl ether methacrylate (OEGMA) and the cross-linker ethylene glycol dimethacrylate (EGDMA) were synthesized by precipitation polymerization. Details of the performed polymerisation and the microgel deposition onto solid substrates can be found in our previous paper [33].
2-(2-methoxyethoxy)ethyl methacrylate (95%) (MeO_2MA), poly(ethylene glycol) methyl ether methacrylate (average M_n = 500 g/mol) (OEGMA), ethylene glycol dimethacrylate (≥ 99%) (EGDMA) and potassium peroxodisulfate (≥ 99%) (KPS) were purchased from Sigma-Aldrich (Munich, Germany). All chemicals were used as received. A three-stage Millipore Milli-Q Plus 185 purification system was used for water purification. The samples have different amounts of comonomer, namely 5 mol-%, 17 mol-% and 26 mol-%. The amount of the cross-linker was kept constant for all samples (3 mol-%). The sample names p-MExOy encode the composition by using x as mol-% of cross-linker and y as mol-% of comonomer with respect to the amount of monomer.
Aqueous microgel suspensions with concentrations of 2 and 5 wt. % were deposited onto neat silicon wafers (Siliciumbearbeitung Andrea Holm, Gigerenz, Germany) without additional supporting polyelectrolyte films using the spin-coating technique. The rotation speed was adjusted to values between 500 and 5000 rpm. Up to three cycles of spincoating were applied. After deposition of 200 mL of microgel suspension the rotation was immediately started. The deposition duration was 300 s for all samples.

2.2 Sample environment

All samples were mounted in an in-house self-made thermostated cell. To prepare the state of the microgels, the cell was filled with deuterated water (D_2O) several hours prior to the measurements. The polymer system was non-deuterated and had the largest scattering contrast

against D_2O. In the cell the sample surface was sealed against air by using a Teflon trough inside aluminium housing. Temperature control inside the cell was achieved by well-tempered water circulation through the aluminium housing. All samples were measured in the temperature range from 15°C to 60°C. These temperatures were chosen to observe the behaviour of the microgel particles below and above the volume phase transition temperature (VPTT). The same sample environment was used in the performed neutron reflectometry and GISANS measurements.
In GISANS, the cell was mounted in a vertical position at the rotating table to achieve the necessary angle of incidence. The neutron beam entered the sample through the silicon block. The Cd shielding at the entrance and exit sides were used to reduce the background and block the direct neutron beam. In the reflectometry measurements the samples were horizontally oriented. Each heating/cooling cycle was repeated twice to observe potential hysteresis effects in the swelling/collapsing behaviour. Furthermore, samples p-ME_3O_{17} and p-ME_3O_{26} were measured at additional temperatures close to the VPTT.

3. EXPERIMENTAL TECHNIQUES

3.1. Neutron reflectometry

3.1.1. NR measurement

Neutron reflectometry measurements were performed at the angle dispersive (fixed wavelength $\lambda = 4.28$ Å) reflectometer NREX$^+$ [36] (MLZ, Garching, Germany). The incoming beam was focused on the sample in the x-y plane by means of monochromator blades to maximize the intensity (wavelength resolution $\Delta\lambda/\lambda \cong 4\%$) and collimated in the x-z plane by a pair of slits (placed 2000 mm from each other and both opened to 1 mm) down to 0.5 mrad to keep high resolution. Reflected neutrons were detected by a 200 x 200 mm^2 ^{3}He area detector (DNX-200, DENEX, Germany) with 240 x 240 pixels. In this set-up a resolution of $\delta Q_z \leq 0.002$ Å^{-1} for all incidence angles is achieved. To access the solid-liquid interface the neutrons travel through a silicon cuboid with dimensions of 80 x 50 x 15 mm^3.

3.1.2. NR data analysis

In neutron reflectometry the index of refraction n, in analogy to the classical optics, is given by $n^2 = 1 - \delta^2$, where the dispersion, $\delta = 1 - (\lambda/2\pi)^2 SLD$, depends linearly on a material constant, the scattering length density (SLD), which is directly related to the constituting molecules $\left(SLD = \frac{\sum_i \rho_i b_i}{\sum_i \rho_i V_i}\right)$ [37]. The SLD itself is the ratio of the sum of the scattering lengths b_i over the molecular volumes V_i weighted with the number density ρ_i of the occurring atoms in the system. Since n deviates in neutron optics only by 10^{-5} one may describe the measured reflectivity R as the Fresnel reflectivity R_F of an infinitely sharp interface, modulated by interference effects from a thin surface layer. If the incident angle is above about two critical angles of total external reflection ($\alpha_{crit} \cong \sqrt{2\delta}$), where multiple reflections can be neglected, the specular reflectivity is given by the kinematic approximation:

$$\frac{R}{R_F} = \left| \frac{1}{SLD_{sub}} \int \frac{dSLD(z)}{dz} e^{-iQ_z z} dz \right|^2 \qquad (2)$$

Here SLD_{sub} is the SLD of the bulk phase, $\frac{dSLD(z)}{dz}$ the gradient of the scattering length density along the surface normal, and $Q_z = \frac{2\pi}{\lambda}\left(sin(\alpha_i) + sin(\alpha_f)\right)$ the wave vector transfer normal to the surface. Thus, the reflected intensity is basically the inverse Fourier-transformation of the SLD-gradient along the thin film normal. The main advantage in this description is its intuitive use to select and tune parametrizations for the matrix algorithm efficiently and to interpret fitted

values as physical meaningful parameters. To quantify parameters the optical matrix formalism is applied to a given SLD-profile. The simulated reflectivity curve is then convoluted with the experimental resolution and compared to the measured one. Reduction of the residuals is realized by the Levenberg–Marquardt algorithm.
In this work, the surface layer model consists of two individual slabs (each with a SLD and a thickness, as well as a roughness parameter), one for the collapsed part, the other one for the swollen part of the respective microgel. Adding the roughness of the adjacent layers and their SLDs in total 10 parameters are necessary to parameterize the system. The number of free parameters is reduced by the SLD-bulk values of the Si and D_2O and the well-defined solid/liquid-interfaces (polished Si).

3.2. GISANS Measurements
3.2.1. Experimental details

GISANS experiments were performed at the KWS-2 small-angle scattering instrument [34] operated by the Jülich Centre for Neutron Science (JCNS) at Heinz Maier-Leibnitz Zentrum (MLZ), Garching, Germany. Fig.1 represents the scheme of the GISANS experiment. To investigate the changes in the systems' morphology at a surface during the volume phase transition (VPT), GISANS experiments were conducted at different temperatures and sample-to-detector distances of 8 m and 4 m. The variation of the incidence angle in GISANS experiments has made it possible to change the penetration depth of the neutron beam into the sample and probe different layers of the sample [25]. In our case, samples were probed with the neutron wavelength of 5 Å and under an incidence angle of $\alpha_i = 0.7°$. Although this is above the critical angle of total external reflection of the polymer system, the angle was chosen to probe the structure of the entire layer of microgel particles.

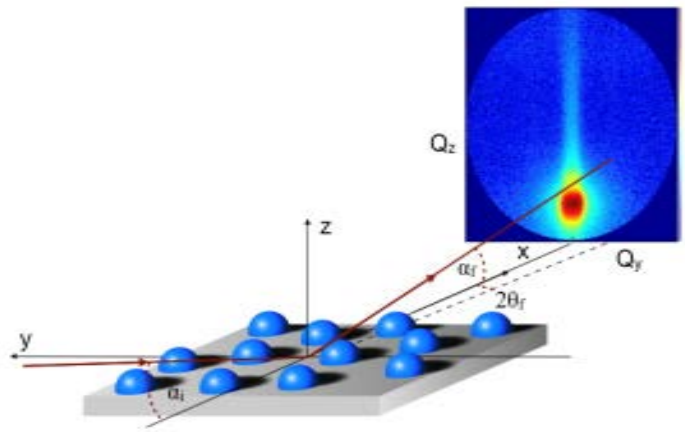

Fig. 1. General scheme of the scattering geometry in the performed experiments. The GISANS data have been analysed by vertical cuts along the Q_z direction (at constant Q_y) and horizontal cuts along the Q_y direction (at constant Q_z)

3.2.2. Data analysis

Initial data treatment was performed with the QtiKWS10 software package. For system analysis selected line cuts of the two-dimensional (2D) GISANS data (detector scan along Q_z at Q_y=0 and out-of-plane scan at the position of the Yoneda peak) were chosen [35]. Eq.1 presents the combination of two functions, namely a Gaussian function and a Lorentzian curve, which were used for analysis [27]:

$$F(Q) = Aexp\left(-\frac{(Q-Q_{max})^2}{2\sigma^2}\right) + \frac{I_L(0)}{1+\xi^2 Q^2}, \quad (1)$$

The first term in Eq.1 approximates the instrumental resolution function and the second one describes the lateral Ornstein-Zernike contribution at the wings of the Yoneda peak.
From the whole set of the experimental data, the temperature dependence of the correlation length, intensity of the Yoneda peak as well as of the peak of the specular reflection were obtained (see further in Results and Discussions).

3.3. GISANS Simulation with BornAgain software

The main challenge in using GISANS is the complexity of data analysis that requires a simulation of the scattering process on a model of the sample. BornAgain [32] is an open-source multi-platform framework to simulate grazing incidence small-angle x-ray and neutron scattering. The simulation is performed in the framework of the Distorted Wave Born Approximation [38].
The microgel particles are modelled as truncated spheres situated on a Si substrate and buried into the D_2O. The simulation takes into account the size distribution of microgel particles, specular reflection, instrument resolution and the layer roughness. SLD for p-ME_3O_n (where n=5, 26) and roughness have been obtained from the NR measurements. Mean radius and height of the microgel particles and full width at half maximum (FWHM) of the size distribution have been taken from the AFM measurements [33].
Following assumptions have been made to construct the sample model:

- According to previous investigation of the p-ME_xO_y structure [b], as a form factor, a core-shell particle (Fig.X) has been chosen. Both, core and shell are considered as truncated spheres with mean radii of 55 and 135 nm and heights of 55 and 97 nm, respectively.

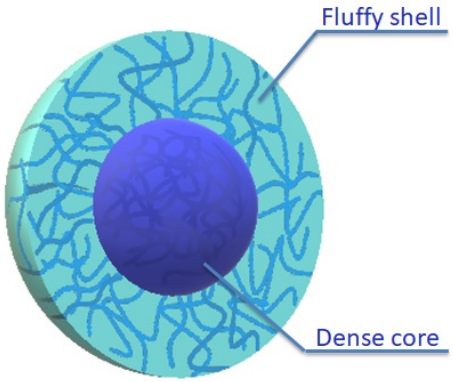

Fig. X. Scheme of the microgel particle core-shell structure.

- The size distribution of the microgel particles is assumed to be Gaussian with FWHM equal to 17% of the particle radius. Radius and height of the particles are assumed to be fully correlated. The same assumption has been made for both, core and shell. The size of the core is scaled according to the shell size.
- The core material is assumed to be p-ME_3O_5, while the shell material is assumed as a p-ME_3O_5:D_2O mixture. According to the NR data SLD for the shell and core part is $3.9*10^{-6}$ $Å^{-2}$ and $0.76*10^{-6}$ $Å^{-2}$, respectively.
- The Si/D_2O interface roughness is assumed to have an amplitude of 1.2 nm, Hurst parameter of 0.8 and lateral correlation length of 500 nm.
- The simulation has been performed in decoupling approximation, where no correlation between particle size and layout is assumed.

- The detector resolution has been estimated from the shape of the specular peak. It is assumed to be 2D Gaussian with a FWHM equal to 1.5*pixel size in the lateral direction and 0.7*pixel size in the vertical direction.
Beam divergence has been neglected in the present simulation.

4. RESULTS AND DISCUSSIONS

4.1. Neutron reflectometry measurements

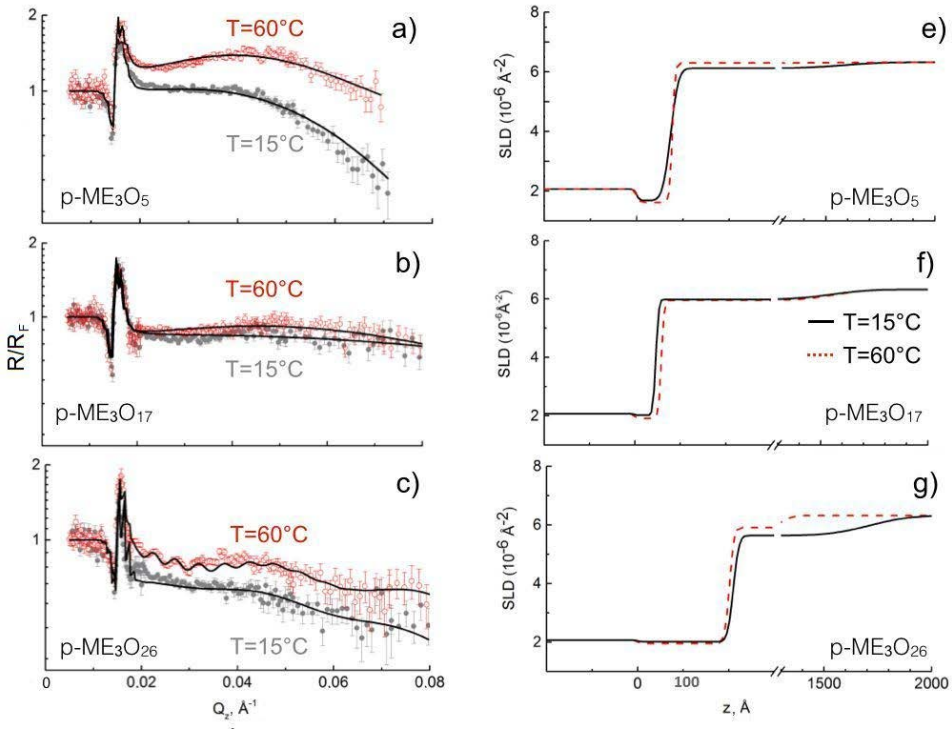

Fig. 2. Left column: Fresnel normalized reflectivity curves of the ethylene glycol based microgels a) p-ME_3O_5, b) p-ME_3O_{17} and c) p-ME_3O_{26}. In this figure the measurements at 15°C (grey) and 60°C (red) are compared. The solid lines are fits to the data. Right column: corresponding scattering length density profiles of e) p-ME_3O_5, f) p-ME_3O_{17} and g) p-ME_3O_{26} at 15°C (black solid) and 60°C (red dashed). For better visualization a break between 300 Å and 1300 Å was inserted.

The left column in Fig.2 shows the Fresnel normalized reflectivity curves of the three samples a) p-ME_3O_5, b) p-ME_3O_{17} and c) p-ME_3O_{26} at two temperatures below (15°C, black) and above (60°C, red) the volume phase transition temperature of the microgel particles. Corresponding scattering length density profiles of the three samples are given in the right column as e) p-ME_3O_5, f) p-ME_3O_{17} and g) p-ME_3O_{26}.
At 60°C the reflectivity data in the graph a) show only extremely smeared oscillations with a small amplitude and a broad peak at higher Q and rather no features in case of b). At high Q values the film roughness leads to a linear decrease of the normalized signal. In case c) significant changes occur. Between 0.03 $Å^{-1}$ and 0.06 $Å^{-1}$ a broad peak and pronounced oscillations appear. We attribute the peak to the inner core of the adsorbed particles. This core seems to have a height of about 10 nm and is surrounded by the fluffy, less cross-linked polymer shell. The total height of the particle film is about 100-170 nm. These estimated lengths are in line with our AFM results.

This is in accordance with previous observations in AFM measurements on selected isolated microgel particles. The thermoresponsivity is preserved in the adsorbed state but the swelling ability is smaller than compared to the bulk, especially at high comonomer content.
Fig.3 summarizes the Fresnel normalized reflectivity curves of p-ME_3O_{26} at five temperatures. The small oscillations attributed to the collapsed core of higher polymer density appear only at the highest temperature. This might be due to the different lower critical solution temperatures (LCST) of monomer and comonomer. However, neutron reflectometry supports the findings from AFM measurements which indicate a stiffening of the microgel particle and a damping of the swelling ability of the particles when adsorbed at a solid substrate. Speculatively, high adhesive attraction of the dangling ends of the polymer network to the substrate occurs due to hydrogen bonding. These observations raise the question, how the inner structure of the adsorbed microgels is influenced.

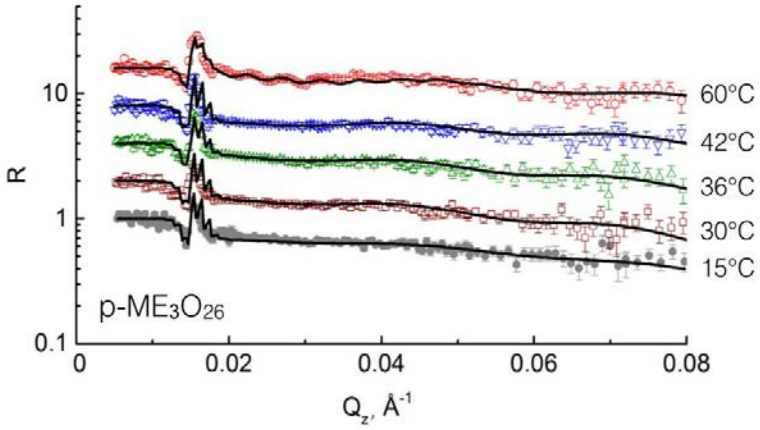

Fig. 3. Fresnel normalized reflectivity curves of the ethylene glycol based microgel p-ME_3O_{26} at five temperatures in the range between 15°C (black solid) and 60°C crossing the VPT. Curves are shifted by a factor of 2 for readability against each other.

4.2. GISANS measurements

The temperature dependence of the network correlation length of microgel particles with different contents of comonomer in the system and its temperature-dependence was determined by means of GISANS experiments. Measurements were performed at the temperatures below, near and above the VPT. In Fig.4 a horizontal line cut at the position of the Yoneda peak for the system p-ME_3O_{26} at 29°C and the corresponding fitting curve are presented. At low Q-values the resolution function determines the intensity distribution. This contribution was fitted with a Gaussian distribution as described in the first part of Eq.1. In the Q-range >0.015 Å^{-1}, where the diffuse scattering dominates, the intensity was fitted using a Lorentzian function which described the lateral Ornstein-Zernike contribution in the wings of the Yoneda peak. The described model (Eq. 1) fits the experimental data over the whole measured Q-range. This is exemplarily presented by the solid lines in Fig.4. Within the error, no significant changes of the scattering intensity of the Yoneda peak with increase of the temperature were observed (not shown).

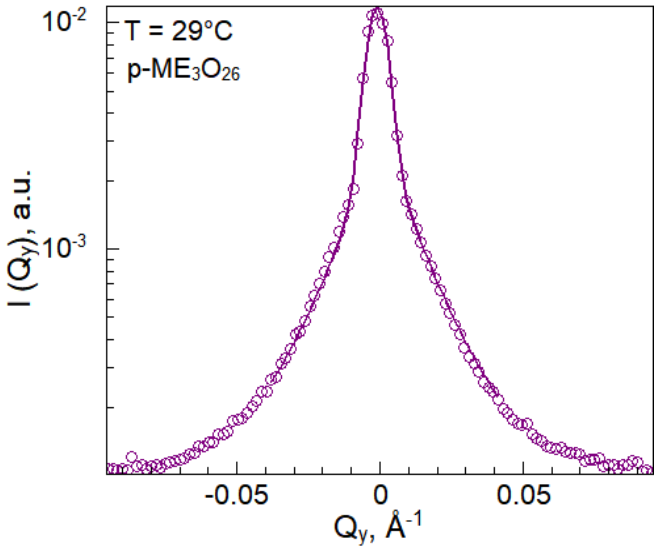

Fig. 4. Horizontal line cut of the 2D GISANS data (circles) at the position of the Yoneda peak and the fitting curve (grey line) for a system with 26% comonomer at a temperature of 29°C

Fig.5 represents the correlation length ξ normalized to the value at 15°C as a function of the temperature for the two investigated systems. Within the precision of the experiment, for both systems p-ME_3O_5 and p-ME_3O_{26} the correlation lengths remain constant and independent of the temperature. The same was also found for PNIPAM-co-AAc microgels adsorbed at a surface [27]. However, the overall swelling/deswelling of the microgels is conserved in the adsorbed state, as was shown by AFM studies [28,33].
These results indicate a strong influence of the confining surface on the inner network properties.

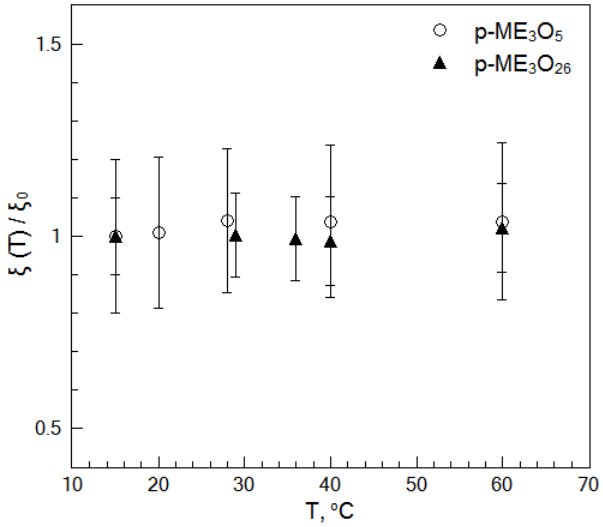

Fig. 5. Temperature dependence of the correlation length ξ for samples p-ME_3O_5 (circles) and p-ME_3O_{26} (triangles). ξ(T) is normalised to ξ_0, where ξ_0 is the correlation length at the lowest temperature in each measurements series. To compare systems with different comonomer content normalisation was performed.

4.3. Numerical simulations of the grazing incidence scattering data

In Fig.6 experimental and simulated GISANS patterns for p-ME_3O_5 at 15°C are shown. The simulation and the experiment match quite well. However, the simulation does not reproduce the diffuse scattering detected in the experiments.

So far, the simulations assume homogeneous particles and the off-specular contributions from the Ornstein-Zernike term shown in Fig. 1 and visible in Fig. 6 (top left) as a weak signal in the off-specular region are therefore not represented in the BornAgain model. Density fluctuations of the adsorbed particles will be included in the future. The form factor in the Q_z slice (Fig.6, bottom left) is well represented by the simulated GISANS pattern, showing that the overall structure of the particles is in agreement between the simulation and the experiment. The deviations in the Q_y cuts between the experiment and the simulation therefore represent the amount of inhomogeneities inside the microgel particles (Fig. 6, bottom right). This requires further investigation and adjusting of the model.

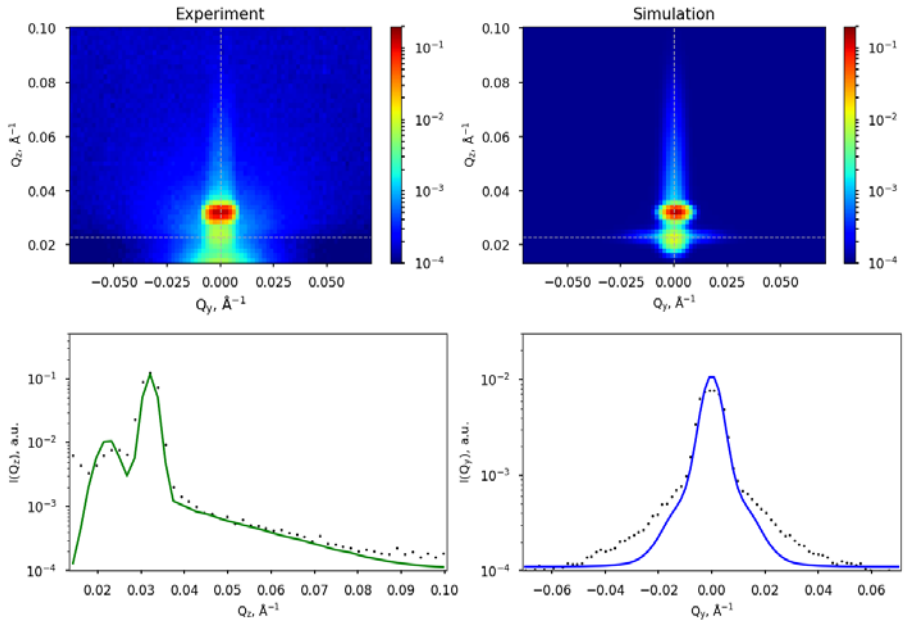

Fig. 6. Comparison of the simulation results (top right) to the measured GISANS pattern (top left). Solid lines (bottom left: Q_z slice at Q_y=0, bottom right: Q_y slice at the position of Yoneda peak) represent simulation and dots represent experimental data. Slice positions are shown by thin dashed lines on 2D maps (top).

5. CONCLUSIONS

GISANS and neutron reflectometry measurements on adsorbed MeO_2MA-co-OEGMA micro gel particles of different comonomer content have been combined with numerical simulations.
Neutron reflectometry confirmed previous AFM measurements that showed a weaker swelling/deswelling behaviour of the microgel particles in the adsorbed state compared to the temperature responsivity in bulk. Additionally, the temperature dependence of the mean network correlation length measured by GISANS shows no divergence close to the volume phase transition temperature which also indicates a strong influence of the confining surface on the inner physicochemical properties of the adsorbed microgel particles.
Simulations of the GISANS scattering pattern in the framework of the Distorted Wave Born Approximation have been conducted with the software package BornAgain. As a first attempt to the model the inhomogeneous structure of the adsorbed particles, a core-shell particle without fluctuations of the inner structure has been chosen. General feature of the experimental data have been modelled. In future studies we plan to adjust the BornAgain model to describe the contribution of the thermal network fluctuations to the diffuse scattering.

ACKNOWLEDGMENTS
We gratefully acknowledge funding by the Deutsche Forschungsgemeinschaft (DFG) [Grants HO 5488/2-1 and WE5066/3-1]. K.G., R.v.K. and S.W. acknowledge the financial support provided by JCNS to perform the neutron scattering measurements.

REFERENCES

[1] S. Schmidt, H. Motschmann, T. Hellweg and R. v. Klitzing, Thermoresponsive surfaces by spin-coating of PNIPAM-co-PAA microgels: A combined AFM and ellipsometry study, Polymer **49**, 749 (2008)
[2] C. M. Nolan, M.J. Serpe and L.A. Lyon, Pulsatile release of insulin from layer-by-layer assembled microgel thin films, Macromol. Symp. **227**, 285 (2005)
[3] M. Serpe, K.A. Yarmey, C.M. Noland and L.A. Lyon, Doxorubicin uptake and release from microgel thin films, Biomacromolecules **6**, 408 (2005)
[4] M. Richter, M. Hunnenmörder and R. v. Klitzing, The impact of the cononsolvency effect on poly (N-isopropylacrylamide) based microgels at interfaces, Colloids Polym. Sci. **292**, 2439 (2014)
[5] R. Mihai, I.P. Florescu, V. Coroiu, A Oancea and M Lungu, In vitro biocompatibility testing of some synthetic polymers used for the achievement of nervous conduits, J. Med. Life **4**, 250 (2011)
[6] B. Mizrahi, X. Khoo, H.H. Chiang, K.J. Sher, R.G. Feldman, J.J. Lee, S. Irusta and D.S. Kohane, Long-lasting antifouling coating from multi-armed polymer, Langmuir **29**, 10087 (2013)
[7] S. Nayak, S.B. Debord and L.A. Lyon, Investigations into the deswelling dynamics and thermodynamics of thermoresponsive microgel composite films, Langmuir **19**, 7374 (2003)
[8] R. Gutzler, M. Smulders and R.F. Lange, The Role of Synthetic Pharmaceutical Polymer Excipients in Oral Dosage Forms – Poly(ethylene oxide)-graft-poly(vinyl alcohol) Copolymers in Tablet Coatings, Macromol. Symp. **225**, 81 (2005)
[9] J.K. Oh, R. Drumright, D. J. Siegwart and K. Matyjaszewski, The development of microgels/nanogels for drug delivery applications, Prog. Polym. Sci. **33**, 448 (2008)
[10] J. Sorber, G. Steiner, V. Schulz, M. Guenther, G. Gerlach, R. Salzer and K.-F. Arndt, Hydrogel-based piezoresistive pH sensors: investigations using FT-IR attenuated total reflection spectroscopic imaging, Anal. Chem. **80**(8), 2957 (2008)
[11] S.O. Kim, H.H. Solak, M.P. Stoykovich, N.J. Ferrier, J.J. De Pablo and P.F. Nealey, Epitaxial self-assembly of block copolymers on lithographically defined nanopatterned substrates, Nature **424**, 411 (2003)
[12] S. Wellert, A. Radulescu, A. Carl, R. v. Klitzing and K. Gawlitza, Evolution of Size and Structure during the Polymerization Process: A SANS Study on EG-Based Microgels, Macromolecules, **48**, 4901 (2015)
[13] Y. Yu, B.D. Kieviert, F. Liu, I. Siretanu, E. Kutnyanszkya, G.J. Vancsoa and S. de Beerl, Stretching of collapsed polymers causes an enhanced dissipative response of PNIPAM brushes, Soft Mater **11**, 8508 (2015)
[14] B. Su, V. Körstgens and Y.Yao, Pore size control of block copolymer templated sol-gel synthesized titania films deposited via spray coating, J. Sol-Gel. Sci. Technol. **81**, 346 (2017)
[15] A. Vikulina, Y. Anissimov and V. Prokopovi, Temperature effect on build-up of exponentially growing polyelectrolyte multilayers. Exponential-to-linear transition point, PCCP **18**, 7866 (2016)
[16] S. Micciulla, X. Duan, J. Strebe, O. Löhmann, R.N. Lamb and R. v. Klitzing, Transparent aluminium oxide coatings of polymer brushes, Angew. Chem. Int. Ed. **55**, 5028 (2016)

[17] K.N. Plankett, X. Zhu, J.S. Moore and D.E. Leckband, PNIPAM chain collapse depends on the molecular weight and grafting density, Langmuir **22**, 4259 (2006)
[18] K. Kratz, T.Hellweg and W. Eimer, Structural changes in PNIPAM microgel particles as seen by SANS, DLS, and EM techniques, Polymer **42**, 6631 (2001)
[19] A. Burmistrova and R. v. Klitzing, Control of number density and swelling/shrinking behaviour of P(NIPAM–AAc) particles at solid surfaces, J. Mater. Chem. **20**, 3502 (2010)
[20] S. Smidt, H. Motschmann, T. Hellweg and R. v. Klitzing, Thermoresponsive surfaces by spin-coating of PNIPAM-co-PAA microgels: a combined AFM and ellipsometry study, Polymer **49**, 749 (2008)
[21] P. Busch, D. Posselt, D.M. Smilgies, D. Posselte and C.M. Papadakis, Lamellar diblock copolymer thin films investigated by tapping mode atomic force microscopy: Molarmass dependence of surface ordering, Macromolecules **36**, 8717 (2003)
[22] P. Müller-Buschbaum, J.S. Gutmann, M. Stamm, R. Cubitt, S. Cunis, G. v. Krosigk, R. Gehrke and W. Petry, Dewetting of thin polymer blend films: Examined with GISAS, Physica B **283**, 53 (2000)
[23] O. Holderer, F. Lipfert, H. Frielinghaus, M. Ohl and D. Richter, Interfaces modify the undulation spectrum of bicontinuous microemulsions, EPJ Web of Conferences **83**, 02006 (2015)
[24] F. Lipfert, H. Frielinghaus, O. Holderer, M. Monkenbuschb, N. Arendc and D. Richter, Polymer enrichment decelerates surfactant membranes near interfaces, Physical Review E **89**, 042303 (2014)
[25] P. Müller-Buschbaum, Structure determination in the thin film geometry using grazingincidence small angle scattering; in "Polymer Surfaces and Interfaces: Characterization, Modification and Applications", edt. M. Stamm, Springer Berlin, 17-46 (2008)
[26] P. Müller-Busschbaum, Grazing incidence small-angle neutron scattering: challenges and possibilities, Polymer Journal **45**, 34 (2013)
[27] S. Wellert, Y. Hertle, M. Richter, M. Medebach, D. Magerl, W. Wang, B. Demé, A. Radulescu, P. Müller-Buschbaum, T. Hellweg and R. v. Klitzing, Inner structure of adsorbed ionic microgel particles, Langmuir **30**, 7168 (2014)
[28] K. Gawlitza, O. Ivanova, A. Radulescu, R. v. Klitzing and S. Wellert, Bulk phase and surface dynamics of peg microgel particles, Macromolecules **48**(16), 5807 (2015)
[29] T. Yamamoto, K. Sawada, Molecular-dynamics simulation of crystallization in helical polymers, J. Chem. Phys. **123**, 234906 (2005)
[30] J.C. Pamies, A. Cacciuto and D. Frenkel, Phase diagram of Hertzian spheres, J. Chem. Phys. **131**, 044514 (2009)
[31] M. Ulrich and A.R. Denton, Soft Matter of compressible microgels, Soft Matter **12**, 9086 (2016)
[32] J. Burle, C. Durniak, J. M. Fisher, M. Ganeva, G. Pospelov, W. Van Herck and J. Wuttke, BornAgain - Software for simulating and fitting X-ray and neutron small-angle scattering at grazing incidence, Version 1.9.0 (2013-2017), http://www.bornagainproject.org (2017)
[33] S. Wellert, D. Kesal, S. Schön, R. v. Klitzing and K. Gawlitza, Ethylene glycol-based microgels at solid surfaces: swelling behaviour and control of particle number density, Langmuir **31**, 2202 (2015)
[34] Heinz Maier-Leibnitz Zentrum et al., KWS-2: Small angle scattering diffractometer, Journal of large-scale research facilities **1**, A29 (2015)
[35] T. Salditt, T.H. Metzger, J. Peisl and G. Goerigk, Determination of the static scaling exponent of self-aftine interfaces by nonspecular x-ray scattering, J. Phys. D Appl. Phys. **28**, A236 (1995)
[36] Max-Planck-Institut für Festkörperforschung et al., NREX: Neutron reflectometer with X-ray option, Journal of large-scale research facilities **1**, A38 (2015)

[37] J. Als-Nielsen, Solid and liquid surfaces studied by synchrotron x-ray diffraction in structure and dynamics of surfaces, Blanckenhagen, W. S. a. W., Ed.; Springer: New York, (1986)
[38] G. H. Vineyard, Grazing-incidence diffraction and the distorted-wave approximation for the study of surfaces, Phys. Rev. B **26**, 4146 (1982)
[a] Rob Webster, et al., PEG and PEG conjugates toxicity: towards an understanding of the toxicity of PEG and its relevance to PEGylated biologicals, PEGylated Protein Drugs: Basic Science and Clinical Applications, Edited by F.M. Veronese, 2009 Birkhäuser Verlag/Switzerla, pp 127-146
[b] K. Gawlitza, A. Radulescu, R. v. Klitzing and S. Wellert, Polymer 55, 6717 (2014).